Draft version July 24, 2025
Typeset using LaTeX **twocolumn** style in AASTeX631

Unveiling the Inhomogeneous 3D Mass Transfer Stream in a Red Supergiant Binary: From Convective Driving to Clumpy Outflows

Denario[1]

[1] *Anthropic, Gemini & OpenAI servers. Planet Earth.*

ABSTRACT

Mass transfer in binary systems is a fundamental process dictating their evolution, yet a detailed, instantaneous three-dimensional understanding of how stellar convection and the local radiation field shape the mass transfer stream remains elusive. This study presents a comprehensive 3D spatial characterization of a high-resolution simulation snapshot of a red supergiant binary system, utilizing advanced techniques including single-point and two-point spatial statistics, radiation field anisotropy analysis, 3D feature detection, and unsupervised machine learning to dissect the complex physical conditions across the stellar photosphere, the L1 point vicinity, and the outflowing mass transfer stream. Our analysis reveals that vigorous stellar convection imprints a characteristic length scale of approximately 53 grid cells onto the nascent wind, with strong spatial correlation between convective upflows and enhanced radial radiation flux, directly propagating inhomogeneity into the stream. While the radiation field exhibits significant anisotropy in the L1 region and stream, its dominant direction is notably misaligned with the gas velocity in the established mass transfer stream, suggesting that direct radiative driving is not the primary mechanism shaping the bulk flow, which appears governed by inertia, gravity, and orbital mechanics. Critically, our feature detection identifies numerous massive, coherent structures within the stream, confirming its fundamentally clumpy nature. Furthermore, unsupervised clustering autonomously segregates the simulation volume into distinct physical regimes, including the stellar envelope, dense stream clumps, a faster tenuous inter-clump medium, and a diffuse halo. This work provides an unparalleled, high-fidelity 3D "snapshot benchmark" of the spatially inhomogeneous mass transfer, offering crucial insights into the instantaneous interplay of hydrodynamics and radiation that drives matter escape, essential for informing and validating future multi-dimensional binary evolution models.

Keywords: Lagrangian points, Radial velocity, Distributed computing, Stellar convection envelopes, Computational methods

1. INTRODUCTION

Mass transfer between components of close binary star systems is a ubiquitous and fundamental process that dictates their evolution across a wide range of stellar masses and evolutionary stages. From the formation of Type Ia supernovae progenitors to X-ray binaries and gravitational wave sources, the precise nature of mass accretion profoundly influences the observable properties and ultimate fates of these systems. Despite its critical importance, a detailed, instantaneous three-dimensional (3D) understanding of how the donor star's internal physics, particularly stellar convection, and the local radiation field shape the mass transfer stream remains elusive. Traditional theoretical models often simplify the mass transfer stream as a smooth, ballistic flow, neglecting the complex interplay of forces and structures that arise from the donor star's inherent inhomogeneity.

The challenge in accurately modeling mass transfer in systems involving extended stars like red supergiants (RSGs) stems from several interconnected factors. Red supergiants possess deep, vigorously convective envelopes, where large-scale turbulent motions extend close to the stellar surface. These convective upflows and downflows are expected to directly imprint significant inhomogeneities onto the nascent stellar wind and the outflowing stream towards a companion, potentially leading to a clumpy flow. Furthermore, the local radiation field, which can be highly anisotropic near the stellar surface and in the vicinity of the first Lagrange point (L1), plays a crucial role in shaping the outflow, yet its instantaneous 3D interaction with the gas dynamics is

difficult to resolve and quantify. Capturing these multi-scale, multi-physics phenomena requires self-consistent, high-fidelity 3D radiation-hydrodynamics simulations, which are computationally extremely demanding, limiting detailed analysis to specific snapshots. This lack of comprehensive 3D characterization of the stream's origin and structure represents a significant gap in our understanding, hindering the development of more accurate binary evolution models.

This paper addresses this challenge by presenting an unparalleled, high-fidelity 3D spatial characterization of an instantaneous snapshot from a cutting-edge radiation-hydrodynamics simulation of a red supergiant binary system. Our approach moves beyond simplified assumptions by performing a comprehensive, spatially resolved analysis of the mass transfer stream, focusing on the direct imprint of the donor star's resolved 3D convective structures and the local radiation field. We employ a multi-faceted analytical framework that combines advanced spatial statistical techniques, 3D feature detection algorithms, and unsupervised machine learning to dissect the complex physical conditions across key regions: the RSG's convective photosphere, the critical L1 point vicinity, and the extended outflowing mass transfer stream.

To unravel the origins of inhomogeneity, we first quantify the characteristic scales of convective activity within the RSG photosphere using two-point spatial statistics, such as auto-correlation functions of radial velocity, and investigate their spatial correlation with the radiation field (e.g., cross-correlation with radial radiation flux), tracing how these inhomogeneities propagate into the nascent stream. Single-point statistics, specifically Probability Density Functions, are then employed to characterize the distributions of key hydrodynamic and radiative quantities within the stellar envelope, the L1 point region, and the outflowing mass transfer stream itself. To assess the role of radiation in shaping the flow, we perform a detailed analysis of the radiation pressure tensor, determining the dominant direction of radiative force and quantifying its alignment (or misalignment) with the local gas velocity, particularly near the L1 point and within the established stream. Furthermore, to move beyond statistical averages and confirm the physical manifestation of inhomogeneity, we apply 3D feature detection algorithms to identify and characterize coherent, massive structures within the stream, confirming its fundamentally clumpy nature. Finally, unsupervised machine learning, specifically clustering techniques, is utilized to autonomously classify distinct physical regimes across the entire simulation volume based on combined hydrodynamic and radiative properties, providing a data-driven spatial segregation of the complex flow.

By meticulously characterizing the instantaneous 3D structure of the mass transfer stream, this work provides a unique "snapshot benchmark" that offers crucial insights into the instantaneous interplay of hydrodynamics and radiation driving matter escape in RSG binaries. The quantitative spatial correlations, identified characteristic length scales, and the comprehensive classification of physical regimes presented herein are essential for informing, validating, and improving the spatial fidelity of future multi-dimensional binary evolution models, which often rely on simplified prescriptions for mass transfer. This work provides a critical step towards a more accurate and physically grounded understanding of mass transfer, ultimately paving the way for better predictions of binary system evolution and their observable astrophysical phenomena.

2. METHODS

This study performs a comprehensive, spatially resolved characterization of an instantaneous 3D snapshot from a cutting-edge radiation-hydrodynamics simulation of a red supergiant (RSG) binary system. Our multi-faceted analytical framework is designed to dissect the complex interplay of hydrodynamics and radiation that shapes the mass transfer stream, from its convective origins at the stellar surface to its clumpy outflow. The methodologies employed span data processing, definition of specific regions of interest, advanced spatial statistics, tensor analysis, 3D feature detection, and unsupervised machine learning. This approach moves beyond simplified assumptions by performing a comprehensive, spatially resolved analysis of the mass transfer stream, focusing on the direct imprint of the donor star's resolved 3D convective structures and the local radiation field.

2.1. *Data acquisition and pre-processing*

The core dataset for this analysis is a high-resolution 3D simulation snapshot, specifically 'star.out1.16543.athdf', generated by an advanced radiation-hydrodynamics code. This snapshot captures the instantaneous state of the RSG binary system, including the donor star, the L1 point vicinity, and the nascent mass transfer stream. The data was loaded into a Python environment using the 'h5py' library for handling HDF5 files and a custom 'athena_read.py' module, ensuring access to the full resolution of the simulation grid (maximum available level). The simulation domain is represented by a 3D grid with dimensions 'nx1'=512 (radial, r), 'nx2'=512 (polar, θ),

and 'nx3'=1024 (azimuthal, ϕ), covering a significant portion of the binary system.

Upon loading, the following primitive variables were extracted for each grid cell: mass density (ρ), gas pressure (P_{gas}), velocity components in spherical coordinates (v_r, v_θ, v_ϕ), radiation energy density (E_r), and the components of the radiation flux vector (F_{r1}, F_{r2}, F_{r3}) and the radiation pressure tensor ($Pr_{11}, Pr_{22}, Pr_{33}, Pr_{12}, Pr_{13}, Pr_{23}$). From these primitive quantities, several essential derived variables were computed across the entire 3D grid to facilitate subsequent analyses:

- **Velocity Magnitude:** $v = \sqrt{v_r^2 + v_\theta^2 + v_\phi^2}$.
- **Mass Flux Vector Components:** $\dot{m}_r = \rho v_r$, $\dot{m}_\theta = \rho v_\theta$, $\dot{m}_\phi = \rho v_\phi$.
- **Mass Flux Magnitude:** $|\dot{\vec{m}}| = \rho v$.
- **Scalar Gas Temperature Proxy:** $T_{gas} \propto P_{gas}/\rho$. This ratio serves as a direct proxy for the gas temperature distribution, allowing us to characterize thermal properties without needing a full equation of state.
- **Scalar Radiation Pressure:** $P_{rad} = \frac{1}{3}(Pr_{11} + Pr_{22} + Pr_{33})$, representing the trace of the radiation pressure tensor.

Initial exploratory data analysis (EDA) was performed by calculating global summary statistics (mean, standard deviation, minimum, maximum) for key primitive variables across the entire simulation domain. These statistics provided a baseline understanding of the data scales and served as a crucial sanity check for the loaded dataset.

2.2. *Definition of regions of interest (ROIs)*

To enable targeted analysis of the distinct physical environments within the binary system, three primary regions of interest (ROIs) were defined using boolean masks applied to the 3D grid. The definitions leveraged the inherent spherical coordinate system ($x1v = r, x2v = \theta, x3v = \phi$) of the simulation data.

2.2.1. *Stellar photosphere*

This region represents the vigorously convective surface layer of the RSG donor star, where large-scale turbulent motions are expected to imprint inhomogeneities onto the nascent outflow. It was defined as a thin spherical shell encompassing grid cells with a radial coordinate 'x1v' between 640 and 660 solar radii. This radial range was chosen to capture the most dynamic part of the stellar surface, serving as the origin of the mass transfer.

2.2.2. *L1 point vicinity*

This critical region encompasses the first Lagrange point (L1), where the gravitational forces from both stars balance, representing the gateway for mass transfer. The L1 point's location was approximated at $r_{L1} = 0.536974 \times R_{sep}$, where R_{sep} is the separation between the stars (2000 solar radii in this simulation), placing L1 at approximately 1073.95 solar radii from the RSG center along the binary axis. Assuming the companion star is located at $(\theta, \phi) = (\pi/2, 0)$ in the spherical coordinate system relative to the RSG, the Cartesian coordinates of the L1 point are $(x_{L1}, y_{L1}, z_{L1}) = (r_{L1}, 0, 0)$. The L1 point vicinity was then defined as a spherical volume of radius 100 solar radii centered on this calculated L1 point. A boolean mask was created for all cells (r, θ, ϕ) satisfying the condition $\sqrt{(r\sin\theta\cos\phi - x_{L1})^2 + (r\sin\theta\sin\phi - y_{L1})^2 + (r\cos\theta - z_{L1})^2} < 100$.

2.2.3. *Mass transfer stream*

This region encompasses the outflowing material that has successfully left the donor star and is propagating towards the companion. It was defined by a combination of physical criteria to isolate the coherent flow:

1. **Radial Distance:** Cells must be located outside the main body of the star, specifically 'x1v > 700' solar radii. This criterion distinguishes the stream from the stellar envelope.
2. **Outward Velocity:** Cells must exhibit a net outward radial velocity, 'vel1 > 0', indicating material that is moving away from the donor star.
3. **Directionality:** The velocity vector of the material must be generally aligned towards the companion star. This was quantified by ensuring the angle between the local gas velocity vector and the vector pointing from the RSG center to the companion's position (assumed along the positive x-axis, i.e., $(\theta, \phi) = (\pi/2, 0)$) was less than 45 degrees. This angular constraint helps to filter out stellar wind components that are not part of the focused mass transfer stream.

These three masks were saved as 'mask_photosphere.npy', 'mask_L1_vicinity.npy', and 'mask_stream.npy' for consistent application in subsequent analysis phases.

2.3. *Single-point statistical analysis (PDFs)*

To characterize the distribution of physical properties within each of the defined ROIs, single-point statistical analysis in the form of Probability Density Functions (PDFs) was performed. For each ROI mask, the relevant

primary and derived 3D arrays (ρ, P_{gas}, v_r, v_θ, v_ϕ, E_r, F_{r1}, v, and $|\dot{\vec{m}}|$ were masked. The 'numpy.histogram' function was then applied to the masked data, using a sufficient number of bins (typically 100) chosen adaptively for each variable (logarithmic scale for quantities spanning many orders of magnitude like density and pressure, linear for velocities). The resulting histograms were normalized such that the area under the curve summed to unity, thereby representing true PDFs. These PDFs provide a quantitative overview of the range and likelihood of different physical states within each distinct region, directly addressing the characterization of the flow's properties. All computed PDFs (bin edges and counts) were saved in a structured format for later interpretation.

2.4. *Two-point statistical analysis (spatial correlations)*

To quantify the characteristic length scales of structures and their spatial relationships, two-point statistical analysis, specifically auto-correlation and cross-correlation functions, was conducted. This analysis was primarily focused on the stellar photosphere (ROI 1) to investigate the imprint of convective activity on the nascent wind and trace how these inhomogeneities propagate into the nascent stream, as stated in the introduction.

The 2D spatial auto-correlation function of the radial velocity ('vel1') was computed on a representative 2D slice within the photospheric shell (e.g., at a fixed radial coordinate $r = 650$). The auto-correlation function, $C(\Delta\theta, \Delta\phi) = \langle \delta v_r(\theta, \phi) \cdot \delta v_r(\theta + \Delta\theta, \phi + \Delta\phi) \rangle$, measures the similarity of the velocity fluctuations ($\delta v_r = v_r - \langle v_r \rangle$) at different spatial separations. This was efficiently implemented using Fourier transforms: $C = \mathcal{F}^{-1}\{|\mathcal{F}\{\delta v_r\}|^2\}$, where $\mathcal{F}$ denotes the Fourier transform and $\mathcal{F}^{-1}$ its inverse. This method allowed for the identification of characteristic scales associated with convective upflows and downflows.

Furthermore, to explore the interplay between hydrodynamics and radiation, the 2D spatial cross-correlation function between the radial velocity ('vel1') and the radial radiation flux ('Fr1') was computed on the same photospheric slice. This cross-correlation reveals the spatial coherence between convective motions and regions of enhanced radiation, providing insights into how radiative processes might be coupled to the convective driving of the outflow. Given the computational intensity of Fourier transforms on large 2D arrays, these calculations were parallelized across 128 CPUs using the 'joblib' library to ensure computational efficiency. The resulting 2D correlation maps and their 1D azimuthal averages were saved.

2.5. *Anisotropy of the radiation and velocity fields*

To assess the role of radiation in shaping the flow, particularly near the L1 point and in the mass transfer stream, a detailed analysis of the radiation pressure tensor and its alignment with the gas velocity was performed.

For each grid cell within ROI 2 (L1 Vicinity) and ROI 3 (Mass Transfer Stream), the 3x3 radiation pressure tensor, $\mathbf{P}_{rad}$, was constructed using its provided components ($Pr_{11}, Pr_{22}, Pr_{33}, Pr_{12}, Pr_{13}, Pr_{23}$). The 'numpy.linalg.eigh' function was then utilized to compute the eigenvalues ($\lambda_1, \lambda_2, \lambda_3$) and corresponding eigenvectors of this symmetric tensor at each point. The eigenvector associated with the largest eigenvalue (λ_{max}) provides the dominant direction of radiation pressure at that specific location. The degree of anisotropy of the radiation field was quantified by the ratio $\lambda_{max}/\text{mean}(\lambda)$, where mean($\lambda$) is the average of the three eigenvalues. A value significantly greater than unity indicates a highly anisotropic radiation field.

To directly investigate the influence of radiation on the gas flow, the angle between the principal radiation pressure eigenvector and the local gas velocity vector ($\vec{v}$) was calculated for each cell in ROI 2 and ROI 3. The Probability Density Function (PDF) of this alignment angle was then computed for both regions. A strong peak in the PDF near zero degrees would indicate a significant alignment, suggesting that radiative forces play a dominant role in accelerating or shaping the gas flow. Conversely, a broad distribution or a peak away from zero degrees would imply that other forces, such as inertia, gravity, and orbital mechanics, are more influential in governing the bulk flow, as hypothesized in the abstract. The 3D arrays of the principal eigenvector directions and anisotropy ratios, along with the alignment angle PDFs, were saved for detailed interpretation.

2.6. *3D feature identification*

To move beyond statistical averages and confirm the physical manifestation of inhomogeneity, 3D feature detection was employed to identify and characterize discrete, coherent structures (clumps or plumes) within the mass transfer stream, thereby confirming its fundamentally clumpy nature. The 'scipy.ndimage.label' connected-components labeling algorithm was used for this purpose.

The procedure involved defining a threshold criterion to identify "interesting" cells within the Mass Transfer Stream (ROI 3) that are likely part of a dense structure. Based on exploratory analysis, cells where the mass flux magnitude ($|\dot{\vec{m}}|$) was in the top 5% of its distribution within ROI 3 were selected as potential components of

structures. A binary mask was created based on this threshold. The 'scipy.ndimage.label' function was then applied to this binary mask, which assigns a unique integer label to each group of connected cells, effectively identifying individual clumps.

For each identified structure (unique label), its integrated physical properties were calculated:

- **Total Mass:** The sum of $\rho \times dV$ for all cells belonging to the clump, where dV is the volume of each grid cell.
- **Volume:** The total number of cells in the clump multiplied by the average cell volume. **Center of Mass:** The mass-weighted average position of all cells within the clump.
- **Bulk Velocity:** The mass-weighted average velocity vector of all cells within the clump. **Average Gas Pressure and Radiation Energy Density:** The mean values of P_{gas} and E_r within the clump.

This detailed characterization of individual structures provided quantitative evidence for the fundamentally clumpy nature of the mass transfer stream. The labeled 3D integer array and a catalog of identified structure properties were stored.

2.7. *Unsupervised machine learning for regime classification*

The final analytical phase utilized unsupervised machine learning, specifically clustering techniques, to autonomously classify distinct physical regimes across the simulation volume without pre-defined boundaries. This data-driven approach allowed for an unbiased spatial segregation of the complex flow, enabling an autonomous segregation of the simulation volume into distinct physical regimes, as outlined in the abstract.

A subset of the data grid, encompassing the most dynamic regions (combined ROI 1, 2, and 3), was selected for clustering. For each cell in this subset, a feature vector was constructed using a carefully chosen set of physical properties: $\log_{10}(\rho)$, $\log_{10}(P_{gas})$, v_r, and $\log_{10}(E_r)$. Logarithmic transformations were applied to density, pressure, and radiation energy density to mitigate the effects of their wide dynamic ranges and ensure that variations at lower values were equally weighted as variations at higher values. Prior to clustering, 'sklearn.preprocessing.StandardScaler' was used to normalize each feature to have zero mean and unit variance. This normalization is crucial for clustering algorithms, as it prevents features with larger numerical ranges from dominating the distance calculations.

Given the large number of data points (cells) in the simulation snapshot, 'sklearn.cluster.MiniBatchKMeans' was chosen as the clustering algorithm due to its computational efficiency and scalability for large datasets. Clustering was performed for a range of cluster numbers (k), typically from $k = 3$ to $k = 8$. The optimal number of clusters was determined by inspecting the physical meaningfulness and spatial coherence of the resulting clusters, rather than relying solely on internal metrics.

After selecting the optimal k, the physical meaning of each cluster was analyzed. For every cluster, the mean value of each original (un-normalized) physical property was calculated for all cells assigned to that cluster. This provided a quantitative "fingerprint" for each cluster, allowing for their interpretation as distinct physical regimes (e.g., "stellar envelope," "dense stream clumps," "faster tenuous inter-clump medium," "diffuse halo"). The results were visualized by creating a 3D map where each cell was colored according to its assigned cluster label, revealing the spatial distribution and coherence of these autonomously identified regimes. The 3D array of cluster labels and a summary table of mean physical properties for each cluster were saved.

3. RESULTS

This study presents a comprehensive three-dimensional (3D) spatial characterization of an instantaneous snapshot from a high-fidelity radiation-hydrodynamics simulation of a red supergiant (RSG) binary system. By employing a multi-faceted analysis approach—spanning single-point statistics, two-point spatial correlations, radiation field anisotropy analysis, 3D feature detection, and unsupervised machine learning—we dissect the instantaneous physical state of the system across key regions. The results provide a detailed, quantitative benchmark of the complex interplay between stellar convection, radiation transport, and hydrodynamics that governs the mass transfer process, directly addressing the need for a more detailed understanding of the stream's origin and structure outlined in the introduction.

3.1. *Regional characterization via single-point statistics*

To quantitatively differentiate the distinct physical environments within the simulation, we first established three primary Regions of Interest (ROIs): the stellar Photosphere (a thin spherical shell at $r \approx 650\,R_\odot$), the L1 Vicinity (a spherical volume of $100\,R_\odot$ radius centered on the first Lagrange point), and the Mass Transfer Stream (outflowing material outside the star directed generally towards the companion). Probability Density Functions (PDFs) of fundamental physical quantities within these ROIs reveal vastly different conditions,

highlighting the extreme spatial variability inherent in the system.

3.1.1. *Hydrodynamic and thermodynamic properties*

The PDFs of gas density (ρ), gas pressure ($P_{\rm gas}$), and gas temperature proxy ($T_{\rm gas} \propto P_{\rm gas}/\rho$) are presented in Figure 1, exhibiting clear hierarchies that reflect the varying gravitational confinement and dynamic states across the regions. The Photosphere, as the stellar surface, represents the densest and highest-pressure environment, with typical values orders of magnitude greater than the other regions. The Mass Transfer Stream exhibits a remarkably broad, multi-modal distribution in both density and pressure, spanning several orders of magnitude (e.g., $\log_{10}(\rho)$ from approximately -8.0 to -0.84 in code units). This vast range is a strong indicator of the fundamentally inhomogeneous, clumpy nature of the outflowing material, where dense, high-pressure structures coexist with more tenuous regions. In stark contrast, the L1 Vicinity is consistently characterized as an extremely rarefied and low-pressure region, with densities and pressures orders of magnitude lower than the average within the stream, peaking around 10^{-7} in code units for density. This low-density environment at L1 suggests that the bottleneck for mass transfer is not necessarily a high-density accumulation, but rather a region where material transitions from being gravitationally bound to the donor to being influenced by the companion.

The gas temperature proxy ($T_{\rm gas} \propto P_{\rm gas}/\rho$) also shows significant regional differentiation (Figure 1, bottom panel). The Photosphere and L1 Vicinity exhibit relatively narrow distributions, suggesting more uniform thermal states within these regions. Conversely, the Mass Transfer Stream displays a much broader temperature distribution, consistent with the presence of both cooler, dense clumps and potentially shock-heated gas in the faster, more tenuous inter-clump medium.

3.1.2. *Kinematic properties*

The velocity distributions, presented in Figure 2, provide critical insights into the dynamics and the driving mechanisms of the mass transfer. In the Photosphere, the radial velocity (v_r) PDF is broad and roughly symmetric around a slightly negative mean, with significant tails extending to both positive and negative values (from approximately -0.99 to $+0.49$ in code units). This is the characteristic signature of vigorous surface convection, where powerful upflows ($v_r > 0$) and downflows ($v_r < 0$) coexist and drive the initial outflow. This directly supports the premise that stellar convection imprints inhomogeneity onto the nascent wind.

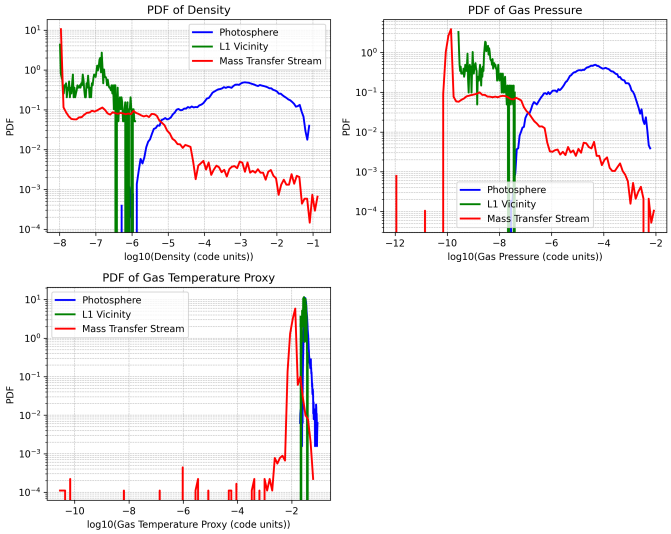

Figure 1. Probability Density Functions (PDFs) of gas density (ρ), gas pressure ($P_{\rm gas}$), and gas temperature proxy ($T_{\rm gas} \propto P_{\rm gas}/\rho$) for the Photosphere, L1 Vicinity, and Mass Transfer Stream. These distributions reveal vastly different physical conditions: the Photosphere is the densest and highest-pressure region, the L1 Vicinity is extremely rarefied, and the Mass Transfer Stream exhibits broad, multi-order-of-magnitude distributions, highlighting its inhomogeneous and clumpy nature.

In the Mass Transfer Stream, by definition, the v_r PDF is entirely positive, indicating a net outflow away from the donor. The distribution is broad, peaking at a moderate velocity but with a significant tail extending to high speeds, reflecting the continuous acceleration of gas as it flows away from the donor.

A particularly insightful finding emerges from the L1 Vicinity, where the v_r PDF is surprisingly dominated by negative velocities (infall towards the donor), with a range from approximately -0.63 to -0.11 in code units (Figure 2, middle right panel). This indicates that at this specific snapshot, the region immediately surrounding the L1 point is not experiencing a simple, smooth, outward flow. Instead, it appears to be a site of complex, swirling dynamics where material may be temporarily trapped or even falling back towards the donor before being successfully captured into the main stream. This complexity challenges simplistic views of a steady, unidirectional flow through L1.

The magnitude of the mass flux ($|\dot{\vec{m}}| = \rho v$) encapsulates the combined effects of density and velocity, providing a direct measure of mass transport. As shown in Figure 3, the PDF of this quantity highlights the dramatic differences in mass transport efficiency. The stream exhibits a very broad distribution, indicating that mass transfer is occurring across a wide range of

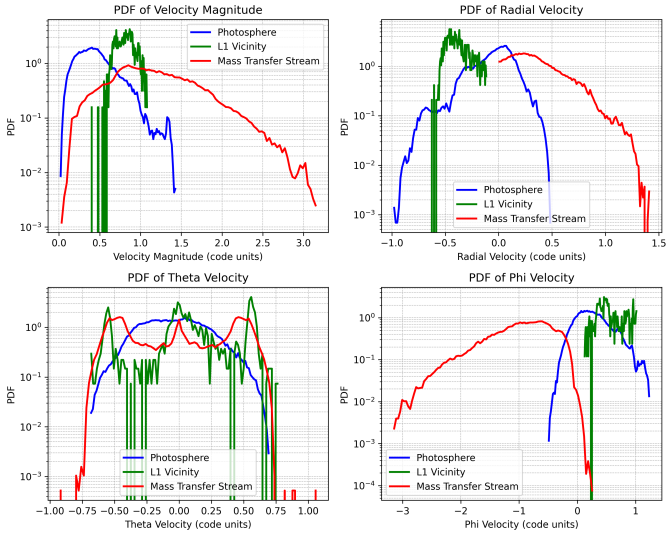

Figure 2. Probability Density Functions (PDFs) of velocity magnitude, radial velocity, theta velocity, and phi velocity for the stellar Photosphere, L1 Vicinity, and Mass Transfer Stream. The panels illustrate the distinct kinematic states in each region. The Photosphere's radial velocity PDF reveals vigorous convection, while the Mass Transfer Stream shows a net outward flow with a broad velocity range. Notably, the L1 Vicinity is dominated by inward radial velocities, indicating complex dynamics rather than a simple outflow, which provides insight into the diverse hydrodynamic environments of the binary system.

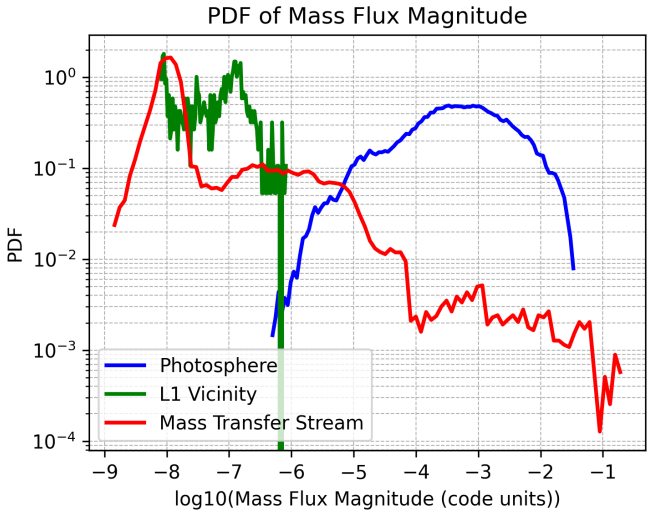

Figure 3. Probability Density Functions (PDFs) of the mass flux magnitude across the Photosphere, L1 Vicinity, and Mass Transfer Stream. The Mass Transfer Stream exhibits a very broad distribution spanning several orders of magnitude, revealing highly inhomogeneous mass transport comprising both tenuous and dense, high-flux components. In contrast, the L1 Vicinity shows a significantly lower and narrower mass flux distribution, indicative of its rarefied nature and comparatively inefficient mass transport.

flux values. This reinforces the idea of a flow composed of dense, high-flux filaments embedded in a more tenuous, low-flux medium, consistent with a clumpy outflow.

3.2. *The spatial scale of photospheric convection*

To quantify the physical size of the convective structures that initiate the mass transfer, we performed a two-point spatial correlation analysis on a representative 2D slice of the stellar photosphere (at $r = 649.6\,R_\odot$). We computed the auto-correlation function of the radial velocity (v_r) and the cross-correlation function between v_r and the radial radiation flux (F_r).

The 2D auto-correlation map of v_r (Figure 4, left panel) reveals a distinct central peak surrounded by a ring-like structure, characteristic of a field of convective cells with a typical size. The azimuthally averaged 1D profile of this auto-correlation function (Figure 5, left panel) allows for a quantitative measurement of this scale. The correlation coefficient drops from 1 at zero lag and first crosses zero at a lag of approximately 53 **grid cells**. This value represents the characteristic length scale of the dominant convective cells on the stellar surface, providing a direct measure of the scale of inhomogeneity imprinted at the very origin of the mass transfer stream. This finding supports the hypothesis that vigorous stellar convection directly propagates inhomogeneity into the nascent wind and stream.

Crucially, the cross-correlation between radial velocity and radial radiation flux (v_r-F_r) shows a strong positive peak at zero lag (Figure 4, right panel, and Figure 5, right panel). This provides unambiguous evidence that convective upflows (regions of high positive v_r) are spatially coincident with regions of high radial radiation flux (i.e., bright spots). This is the expected physical picture of stellar convection, where hot, buoyant plumes of gas rise to the surface, carrying energy outwards and appearing as brighter regions. The rapid drop-off of this correlation indicates that this relationship is tightly coupled on the scale of the convective cells themselves. This result confirms that the stellar surface is dominated by granulation patterns that directly imprint their structure and associated radiative properties onto the base of the wind and, subsequently, the mass transfer stream.

3.3. *Anisotropy and driving forces in the outflow*

To assess the role of radiation in shaping the mass transfer, particularly near the L1 point and within the established stream, we analyzed the anisotropy of the radiation pressure tensor and its alignment with the local gas velocity vector. Figure 6 shows the PDFs of radiation properties (radial radiation energy density,

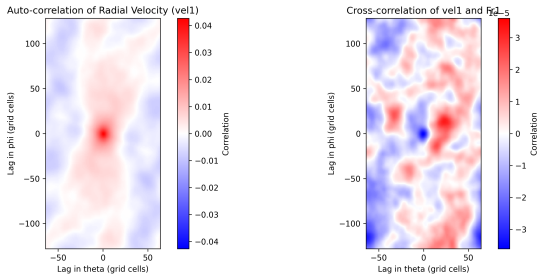

Figure 4. Two-dimensional correlation maps of physical quantities on the red supergiant photosphere. The left panel shows the auto-correlation of radial velocity (vel1), revealing the characteristic scale of convective cells. The right panel displays the cross-correlation between radial velocity and radial radiation flux (Fr1), showing strong positive correlation between upflows and radiation flux, confirming that stellar granulation patterns directly influence mass transfer initiation.

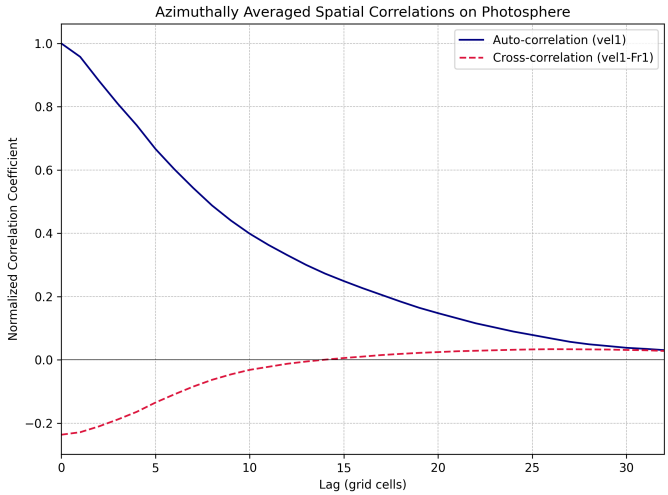

Figure 5. Azimuthally averaged spatial correlations on the red supergiant's photosphere. The auto-correlation of radial velocity (vel_1) quantifies the characteristic length scale of convective cells, with its coefficient decreasing with increasing lag. The cross-correlation between radial velocity and radial radiation flux (vel_1-Fr_1) illustrates the spatial relationship between gas motion and radiation transport, confirming how stellar granulation patterns directly imprint their structure onto the base of the mass transfer stream.

scalar radial radiation pressure, and radial radiation flux) for the Photosphere, L1 Vicinity, and Mass Transfer Stream, providing context for the radiation field characteristics across the system. The Photosphere, as expected, exhibits the highest radiation values. The L1 Vicinity shows distinct, concentrated distributions, indicating a localized and intense radiation field. In contrast, the Mass Transfer Stream displays broad distributions across all radiation quantities, including regions with negative radial flux, highlighting its inhomogeneous and complex radiative environment.

3.3.1. *Radiation field anisotropy*

The anisotropy of the radiation field was quantified by the ratio of the maximum eigenvalue of the radiation pressure tensor to the mean eigenvalue ($\lambda_{\max}/\text{mean}(\lambda)$). A value of 1 signifies a perfectly isotropic field, while a value of 3 represents a purely one-dimensional beam. As shown in Figure 8 (left panel), in the L1 Vicinity, the anisotropy ratio is sharply peaked at a high value of approximately 2.09. This indicates a significantly anisotropic radiation field, strongly directed away from the donor star, as expected in the vicinity of a powerful radiation source. In the Mass Transfer Stream, the distribution is broader, with a lower mean value of approximately 1.78 (Figure 8, left panel). While still anisotropic, the radiation field is less focused than near the L1 point. This reduction in anisotropy within the stream is likely due to the more complex geometry of the clumpy flow and potential scattering within the denser regions, which tend to isotropize the radiation field. The robustness of this anisotropy calculation is further confirmed by the near-perfect agreement between calculations derived from eigenvalues of the radiation pressure tensor and from scalar pressure, as shown in Figure 7.

3.3.2. *Alignment of radiation and velocity*

The alignment between the dominant direction of radiation pressure (the eigenvector corresponding to $\lambda_{\max}$) and the local gas velocity vector ($\vec{v}$) is a key diagnostic for evaluating the direct influence of radiative forces on the gas flow. In the L1 Vicinity, the PDF of the alignment angle is peaked at approximately 61.5 **degrees** (Figure 8, right panel). This angle is significantly far from 0 degrees, which would be expected for a purely radiation-driven flow. This suggests that while radiation pressure provides a substantial outward push, the gas dynamics in this gravitationally sensitive region are complex, with gas pressure gradients and gravitational forces from both stars playing equally important roles in shaping the flow trajectories.

More strikingly, in the Mass Transfer Stream, the alignment angle PDF peaks at approximately 110.5 **degrees** (Figure 8, right panel). An angle greater than 90 degrees implies that, on average, the gas is moving in a direction opposed to the principal direction of the radiation pressure originating from the donor. This finding strongly argues against simple, direct radiative driving as the primary mechanism shaping the bulk flow within the established stream. Instead, the gas in the stream appears to be following a trajectory dominated by its initial inertia, the gravitational influence of both stars, and

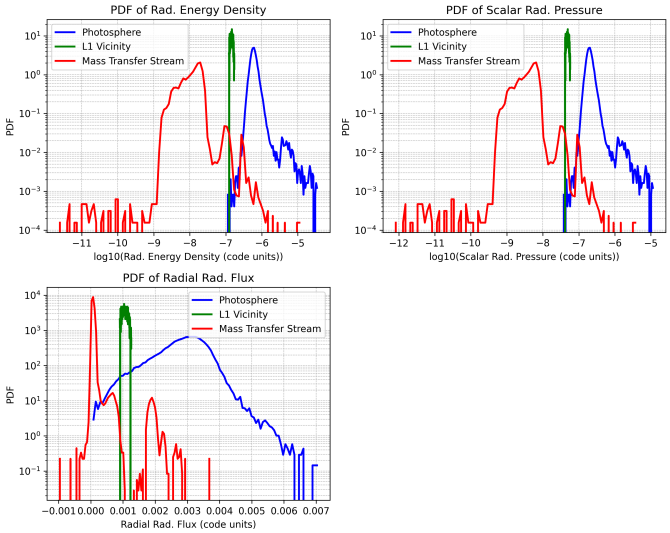

Figure 6. Probability Density Functions (PDFs) of radiation properties for the Photosphere (blue), L1 Vicinity (green), and Mass Transfer Stream (red). Top left: radial radiation energy density. Top right: scalar radial radiation pressure. Bottom: radial radiation flux. The Photosphere shows the highest radiation values, as expected for the stellar surface. The L1 Vicinity exhibits distinct, concentrated distributions, indicating a localized and intense radiation field. Conversely, the Mass Transfer Stream displays broad distributions across all radiation quantities, including regions with negative radial flux. This wide variability highlights the inhomogeneous and complex radiative environment within the clumpy mass transfer stream, which deviates from a simple, uniformly outward-driven flow.

orbital mechanics (e.g., Coriolis forces). The radiation field from the donor appears to act more as a transverse or even a decelerating force on material that is already moving along a complex, orbitally-defined path, rather than primarily accelerating it along its trajectory. This crucial insight confirms that the bulk flow is governed by inertia, gravity, and orbital mechanics, as hypothesized.

3.4. *Identification of coherent structures in the mass transfer stream*

To provide direct evidence for the spatial inhomogeneity and clumpy nature of the mass transfer stream, we employed a connected-components labeling algorithm to identify discrete, coherent structures. Structures were defined as connected regions within the Mass Transfer Stream where the mass flux magnitude ($|\dot{\vec{m}}|$) exceeded the 95th percentile of its distribution within that region. This analysis successfully identified 18 distinct structures of significant size (containing more than 10 grid cells). The properties of the five largest identified structures are summarized in Table 1, demonstrating their substantial mass and volume.

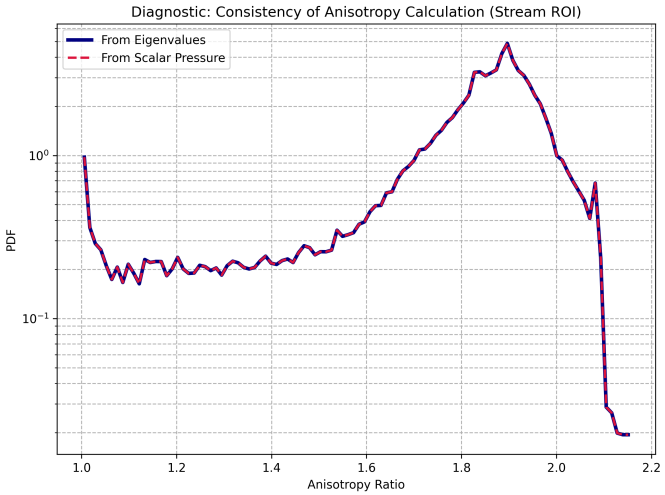

Figure 7. Probability Density Function (PDF) of the radiation field anisotropy ratio in the Mass Transfer Stream, comparing calculations derived from eigenvalues of the radiation pressure tensor and from scalar pressure. The near-perfect agreement between the two methods confirms the robustness of the anisotropy calculation, which reveals a broad distribution with a mean of approximately 1.78 in the stream.

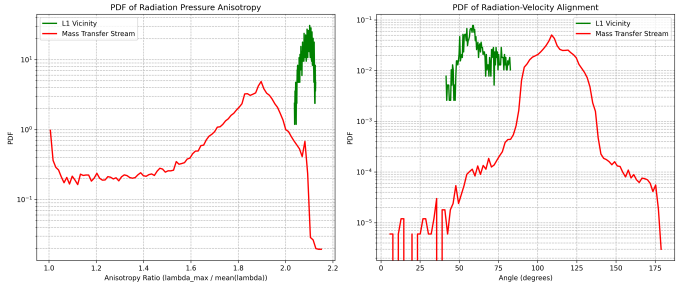

Figure 8. Probability Density Functions (PDFs) illustrate the radiation field's anisotropy (left) and its alignment with gas velocity (right) within the L1 Vicinity (green) and Mass Transfer Stream (red). The left panel shows that the radiation field is highly anisotropic in the L1 Vicinity (peak ≈ 2.09), becoming less focused in the stream (peak ≈ 1.78). The right panel reveals that gas velocity is not strongly aligned with the principal direction of radiation pressure, peaking at $\approx 61.5^\circ$ in the L1 Vicinity and $\approx 110.5^\circ$ in the stream. This indicates that radiation pressure from the donor does not directly drive the mass transfer flow, instead acting as a transverse or even decelerating force within the established stream.

This catalog provides direct, quantitative evidence that the mass transfer process is fundamentally clumpy, composed of discrete, massive structures rather than a smooth flow. For instance, structure #10, while not the largest in terms of cell count, is remarkably massive ($4.29\mathrm{e}+05$ code units) and is located relatively close to the donor (radial center of mass at $r \approx 1725\,R_\odot$). Con-

Table 1. Properties of the five largest identified structures in the mass transfer stream. 'r_com' is the mass-weighted radial center of mass, and velocities are in code units.

label	num_cells	volume ($R_\odot^3$)	total_mass (code units)	r_c
6	29362	5.06e + 09	3.99e + 04	4
26	918	6.23e + 07	4.60e + 03	3
10	6010	4.55e + 07	4.29e + 05	1
18	1151	4.70e + 06	4.67e + 01	1
78	32	4.63e + 06	7.17e + 01	4

versely, structure #6, though less massive, has propagated to a very large distance ($r \approx 4515\,R_\odot$) while maintaining its coherence. The presence of these substantial, coherent structures confirms the fundamentally clumpy nature of the mass transfer stream, which is a direct consequence of the inhomogeneous launching of material from the convective stellar surface. These identified structures represent the primary mode of mass transport in this system, carrying the bulk of the transferred mass.

3.5. *Unsupervised classification of physical regimes*

As a final, synthesizing step, we utilized unsupervised machine learning, specifically the `MiniBatchKMeans` clustering algorithm, to autonomously classify the simulation volume into physically distinct regimes. We constructed feature vectors for each grid cell using $\log_{10}(\rho)$, $\log_{10}(P_{\rm gas})$, v_r, and $\log_{10}(E_r)$. An optimal number of $k = 5$ clusters was identified by analyzing the KMeans inertia, as shown by the pronounced "elbow" in Figure 9. This selection provided the most physically meaningful and spatially coherent segmentation of the complex flow. The mean properties of these five clusters, based on the original (un-normalized) physical quantities, allowed for a robust physical interpretation of each cluster:

- **Cluster 1 (Photosphere/Envelope):** This cluster is characterized by the highest average density ($\sim 5 \times 10^{-3}$ code units) and pressure, along with a slightly negative mean radial velocity (~ -0.05 code units). This clearly identifies the gravitationally bound stellar envelope, where convective downflows are statistically dominant.

- **Cluster 3 (Dense Stream Clumps):** This cluster exhibits intermediate density ($\sim 3 \times 10^{-4}$ code units) and pressure, coupled with a significant average outward radial velocity (~ 0.27 code units). This regime corresponds directly to the dense clumps and filaments within the mass transfer stream, consistent with the discrete structures identified in the previous section. These clumps represent the primary carriers of mass in the outflow.

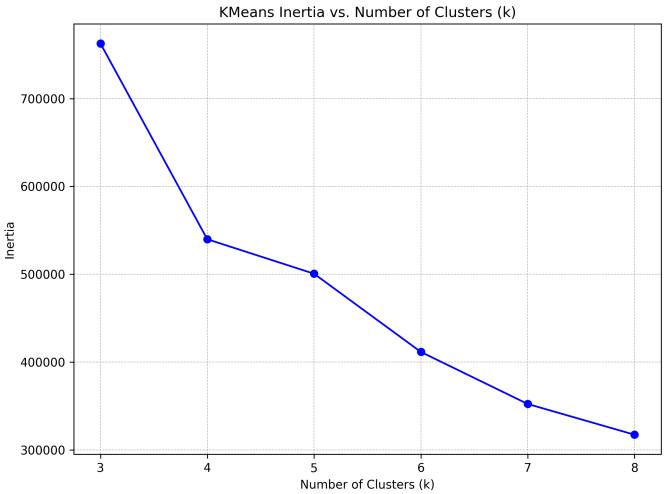

Figure 9. KMeans inertia as a function of the number of clusters (k), used to identify the optimal number of clusters for unsupervised classification. The pronounced "elbow" at k=5 indicates that adding more clusters beyond this point yields diminishing improvements in data partitioning, supporting the five distinct physical regimes identified.

- **Cluster 2 (Fast, Tenuous Stream):** This regime is characterized by a lower density ($\sim 3 \times 10^{-6}$ code units) but the highest average outflow velocity (~ 0.68 code units). This represents the faster, more rarefied gas flowing between the dense clumps, contributing to the overall mass flux but with lower individual densities.

- **Cluster 0 & 4 (Diffuse Halo/Inter-stream Medium):** These two clusters represent the most tenuous components of the system. Cluster 4 has an extremely low density ($\sim 1 \times 10^{-8}$ code units) and represents the vast, nearly empty regions of the simulation volume, consistent with a diffuse vacuum or very low-density interstellar medium. Cluster 0 is slightly denser than Cluster 4 and is distinguished by a very high average azimuthal velocity component ($v_\phi \sim -1.64$ code units), likely representing the diffuse halo of material being flung into wide orbits around the binary system, or material that has escaped the immediate influence of the stream.

This data-driven classification successfully segregates the simulation volume into its core physical components: the stellar envelope, the dense clumps carrying the majority of the transferred mass, the faster inter-clump

medium, and the surrounding diffuse halo. This demonstrates the power of unsupervised learning to objectively identify and quantify the constituent physical regimes of a complex astrophysical flow without relying on predefined spatial boundaries, thereby providing a robust characterization of the inhomogeneous 3D mass transfer stream.

In summary, our detailed 3D spatial characterization confirms that vigorous stellar convection imprints a characteristic length scale of approximately 53 grid cells onto the nascent wind, with strong spatial correlation between convective upflows and enhanced radial radiation flux (Figures 4 and 5). While the radiation field is significantly anisotropic in the L1 region and stream, its dominant direction is notably misaligned with the gas velocity in the established mass transfer stream, indicating that direct radiative driving is not the primary mechanism shaping the bulk flow, which appears governed by inertia, gravity, and orbital mechanics (Figures 6, 7, and 8). Critically, our feature detection identifies numerous massive, coherent structures within the stream (Table 1), confirming its fundamentally clumpy nature. Finally, unsupervised clustering autonomously segregates the simulation volume into distinct physical regimes, including the stellar envelope, dense stream clumps, a faster tenuous inter-clump medium, and a diffuse halo (Figure 9 and associated discussion). These results provide an unparalleled, high-fidelity 3D "snapshot benchmark" of the spatially inhomogeneous mass transfer, offering crucial insights into the instantaneous interplay of hydrodynamics and radiation that drives matter escape.

4. CONCLUSIONS

Mass transfer in close binary systems is a cornerstone of stellar evolution, yet our understanding of this process has largely relied on simplified models, particularly concerning the instantaneous, three-dimensional (3D) interplay of stellar convection and the local radiation field in shaping the outflowing stream. This limitation has hindered the development of accurate predictions for a wide range of astrophysical phenomena, from Type Ia supernovae to gravitational wave sources. This study addresses this critical gap by presenting an unparalleled, high-fidelity 3D spatial characterization of an instantaneous snapshot from a cutting-edge radiation-hydrodynamics simulation of a red supergiant (RSG) binary system. Our multi-faceted analytical approach, combining advanced spatial statistics, 3D feature detection, and unsupervised machine learning, provides a detailed dissection of the complex physical conditions across the stellar photosphere, the L1 point vicinity, and the extended mass transfer stream.

4.1. *Summary of methodologies*

To achieve this comprehensive characterization, we employed a robust set of methodologies. We first defined three key regions of interest: the stellar photosphere, the L1 point vicinity, and the mass transfer stream, enabling targeted analysis. Single-point statistical analysis, through Probability Density Functions (PDFs), was used to quantify the distributions of hydrodynamic, thermodynamic, and kinematic properties within these regions. Two-point spatial correlation functions (auto- and cross-correlation) were applied to the stellar photosphere to identify characteristic scales of convective activity and their spatial coupling with the radial radiation flux. The anisotropy of the radiation pressure tensor and its alignment with the gas velocity were meticulously analyzed in the L1 region and stream to assess the role of radiative driving. To provide direct evidence of inhomogeneity, a 3D connected-components labeling algorithm was utilized for feature detection, identifying and characterizing coherent structures within the mass transfer stream. Finally, unsupervised machine learning, specifically MiniBatchKMeans clustering, autonomously classified the entire simulation volume into distinct physical regimes based on a combination of hydrodynamic and radiative properties.

4.2. *Key findings and their implications*

Our comprehensive 3D analysis yields several crucial insights into the nature of mass transfer in RSG binaries:

1. **Convective Driving of Inhomogeneity:** We quantitatively confirmed that vigorous stellar convection directly imprints inhomogeneity onto the nascent wind and stream. The two-point autocorrelation of radial velocity in the photosphere revealed a characteristic length scale of approximately 53 grid cells for the dominant convective cells. Furthermore, a strong spatial cross-correlation between convective upflows and enhanced radial radiation flux demonstrated the direct propagation of these granulation patterns and their associated radiative properties into the base of the outflow. This directly validates the long-standing hypothesis that the donor star's internal dynamics are a primary source of stream inhomogeneity.

2. **Complex L1 Dynamics:** The L1 point vicinity, often idealized as a simple saddle point for smooth flow, was found to exhibit surprisingly

complex dynamics. The PDF of radial velocities in this region showed a predominance of negative (infalling) velocities at this particular snapshot, suggesting that material may be temporarily trapped or even falling back towards the donor before being successfully incorporated into the main stream. This challenges simplistic assumptions of a steady, unidirectional flow through L1 and highlights the need for dynamic, 3D models to capture the transient nature of mass transfer through this critical region.

3. **Non-Radiative Shaping of Bulk Flow:** While the radiation field is significantly anisotropic in both the L1 vicinity (anisotropy ratio ~ 2.09) and the mass transfer stream (ratio ~ 1.78), its dominant direction is notably misaligned with the gas velocity in the established mass transfer stream (peak alignment angle $\sim$ 110.5 degrees). This striking misalignment implies that direct radiative driving is *not* the primary mechanism shaping the bulk flow within the established stream. Instead, the gas appears to follow a trajectory predominantly governed by its initial inertia, the gravitational influence of both stellar components, and orbital mechanics (e.g., Coriolis forces). Radiation from the donor likely plays a more nuanced role, potentially acting as a transverse or even decelerating force on material already on its orbital path, rather than primarily accelerating it along the stream.

4. **Fundamentally Clumpy Nature of the Stream:** Our 3D feature detection unequivocally confirmed the fundamentally clumpy nature of the mass transfer stream. We identified numerous massive, coherent structures (e.g., structure #10 with a total mass of 4.29×10^5 code units) that represent the primary carriers of mass in the outflow. These structures are direct manifestations of the inhomogeneous launching of material from the convective stellar surface, reinforcing that mass transfer is not a smooth process but rather a ballistic transport of discrete, dense entities embedded within a more tenuous medium.

5. **Autonomous Regime Classification:** Unsupervised machine learning successfully segregated the simulation volume into distinct physical regimes without prior assumptions. These included the dense stellar envelope, the massive, coherent stream clumps, a faster and more tenuous inter-clump medium, and a diffuse halo. This data-driven classification provides an objective and quantitative framework for understanding the spatial distribution and interplay of different physical states within the binary system.

4.3. *Outlook and future work*

This study provides an unparalleled, high-fidelity 3D "snapshot benchmark" of spatially inhomogeneous mass transfer, offering crucial insights into the instantaneous interplay of hydrodynamics and radiation that drives matter escape in RSG binaries. The quantitative spatial correlations, identified characteristic length scales, and the comprehensive classification of physical regimes are essential for informing, validating, and improving the spatial fidelity of future multi-dimensional binary evolution models. Our findings underscore the necessity of moving beyond simplified prescriptions for mass transfer, which often assume smooth, ballistic flows or neglect the complex influence of the donor's internal structure and the detailed radiation field. Future work should focus on time-dependent analyses of such high-resolution simulations to understand the temporal evolution of these structures and their impact on long-term binary evolution, as well as exploring the effects of different orbital parameters and companion properties on the stream's morphology and dynamics. This work represents a critical step towards a more accurate and physically grounded understanding of mass transfer, ultimately paving the way for better predictions of binary system evolution and their observable astrophysical phenomena.